J. Cent. South Univ. (2015) 22: 368−376
DOI: 10.1007/s11771-015-2531-9

Springer

Effects of mesh style and grid convergence on numerical simulation accuracy of centrifugal pump

LIU Hou-lin(刘厚林), LIU Ming-ming(刘明明), BAI Yu(白羽), DONG Liang(董亮)

Research Center of Fluid Machinery Engineering and Technology, Jiangsu University, Zhenjiang 212013, China

Abstract: In order to evaluate the effects of mesh generation techniques and grid convergence on pump performance in centrifugal pump model, three widely used mesh styles including structured hexahedral, unstructured tetrahedral and hybrid prismatic/tetrahedral meshes were generated for a centrifugal pump model. And quantitative grid convergence was assessed based on a grid convergence index (GCI), which accounts for the degree of grid refinement. The structured, unstructured or hybrid meshes are found to have certain difference for velocity distributions in impeller with the change of grid cell number. And the simulation results have errors to different degrees compared with experimental data. The GCI-value for structured meshes calculated is lower than that for the unstructured and hybrid meshes. Meanwhile, the structured meshes are observed to get more vortexes in impeller passage. Nevertheless, the hybrid meshes are found to have larger low-velocity area at outlet and more secondary vortexes at a specified location than structured meshes and unstructured meshes.

Key words: mesh style; grid convergence index (GCI); numerical simulation; particle image velocimetry (PIV); centrifugal pump

1 Introduction

Centrifugal pumps are used in a wide range of applications [1]. Predicting performance of centrifugal pump is of critical importance. To assess pump hydrodynamics, computational fluid dynamics (CFD) analysis has been employed by many researchers [2−4]. CFD simulations are widely employed in industry, and CFD is a developing calculating procedure, so that there is a need to evaluate the uncertainty and error that may be associated with simulation procedures. Verification and validation are the main principles used to determine the credibility of CFD simulation results [5] and the analysis of CFD uncertainty has rarely been applied in centrifugal pump.

Several approaches have been suggested formerly to quantify the uncertainty in numerical simulations [6−9]. Of these, the most commonly used method was developed by ROACHE [8]. He proposed a method for uniform reporting of grid convergence and numerical errors using the grid convergence index (GCI). The GCI is based on generalized Richardson extrapolation [10] and involves the comparison of discrete solutions at two different grid spacings. It is a method of assessing the influence of discretization and iterative convergence errors on a numerical solution. KARIMI et al [11] used GCI to account for numerical uncertainty in a hydrocyclone model. They found that the mesh refinement produced a reduction in the GCI and suggested that the GCI is a useful tool for quantifying numerical uncertainty in CFD simulation. ELSAYED and LACOR [12] adopted GCI to accurately evaluate the numerical uncertainties in the computational results using three grid-density levels for per cyclone, and the calculation results meet the demand of monotonic convergence. LIJO et al [13] calculated GCI for the quantification of numerical uncertainty for duct configurations. It is seen that the asymptotic range is well achieved, and a steady state solution is iteratively converged and the space discretization error is small.

Discretization error, the main source of computational errors, may be defined as the difference between the exact solution of the governing equations and the discretized system [14]. These errors can arise from numerical algorithms, the mesh style and quantity used to discretize the equations, boundary conditions, etc. In this work, errors resulting from the mesh style and quality were interested.

There are three types of meshes: structured mesh,

Foundation item: Projects(51109095, 51179075, 51309119) supported by the National Natural Science Foundation of China, Project(BE2012131) supported by Science and Technology Support Program of Jiangsu Province, China
Received date: 2013−09−30; **Accepted date:** 2014−01−03
Corresponding author: LIU Hou-lin; Tel: +86−13952845080; E-mail: liuhoulin@ujs.edu.cn

unstructured mesh and hybrid mesh. Unstructured tetrahedral meshes can be largely automated by current mesh generation software. These meshes can be refined in regions of interest to provide increased resolution and reduced discretization errors. However, tetrahedral meshes are generally considered to be less accurate than structured hexahedral meshes due to a number of factors including poorer alignment with the primary flow direction and fewer control volume nodes [15]. Recently, hybrid meshes have also been introduced, which are combinations of internal elements surrounded by several layers of pyramid, prism or hexahedral elements on the surface in order to better solve the near-wall flow field.

In several studies, the effects of various meshing styles on solution characteristics, grid convergence, and other parameters were considered either directly or indirectly. While simulating a centrifugal pump, ZHOU et al [16] found that structured meshes had a certain advantage in convergence rate and calculation accuracy compared to unstructured meshes, and flow field distributions are closer to the experimental data in structured meshes than in unstructured meshes. LONGEST and VINCHURKAR [17] evaluated the effects of hexahedral, prismatic and hybrid grid on particle deposition in bifurcating airway models. LIU et al [18] compared CFD simulations of structured and unstructured meshes for an anastomotic vessel connection. Flow fields in the structured model were qualitatively similar to the unstructured model and more vortices were present in the structured model than in the unstructured model. Nevertheless, hybrid meshes are rarely considered compared with structure meshes or unstructured meshes in centrifugal pump system.

The objective of this work was to evaluate the effects of different mesh styles and grid convergence on centrifugal pump performance. In order to achieve this objective, three mesh styles including structured hexahedral, unstructured tetrahedral and hybrid tetrahedral/prismatic meshes were considered for the pump model. To test and verify the simulation results, the particle image velocimetry (PIV) test was applied. Accuracy of the simulations was assessed by comparisons to PIV experimental data. This work was intended to serve as a basis for future improvements in accuracy of centrifugal pump.

2 PIV and performance test

2.1 Geometry of test pump

The model pump constructed for PIV measurements consists of an impeller, a volute and a suction chamber. Owing to the limit of land and to facilitate arrangement of optical system and CCD camera, the central side-inlet for pump was adopted. The impeller was shrouded with six strongly backward curved blades at an exit angle of 40° relative to the tangential direction. The volute was designed using equivalent velocity moment method, featured by rectangular cross sections and logarithmic spiral profile. In order to reduce scattering in PIV measurements, the volute was designed in a square shape. Both the impeller and volute were made of acrylic glass for good optical access. Acrylic glass was homogeneous with no bubbles or impurities. All surfaces of acrylic glass were polished, and its roughness was up to R_a= 3.2 μm. Besides, for reducing background noise, non-testing surfaces of the impeller and volute near the suction chamber were set to be black before assembly. The meridian section of the pump is shown in Fig. 1. The geometric data of the pump are summarized in Table 1.

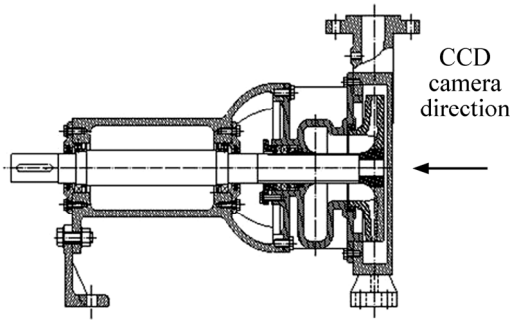

Fig. 1 Meridian section of pump

Table 1 Main geometric parameters of test pump

Parameter	Value
Impeller inlet diameter, D_1/mm	75
Impeller outlet diameter, D_2/mm	200
Blade inlet width, b_1/mm	18
Blade outlet width, b_2/mm	8
Volute base circle diameter, D_3/mm	220
Blade number, Z	6
Blade inlet angle, β_1/(°)	17.6
Blade outlet angle, β_2/(°)	40
Volute outlet width, b_3/mm	11

2.2 Test bench and pump performance results

The performance characteristics test bench is shown in Fig. 2. The inverter control cabinet was used to achieve stepless speed regulation for motor. Electromagnetic flow meter was taken to measure flow. Pressure transmitter was employed to calculate pump head. Three-phase PWM special tester can get power directly. Transmission fluid was water. The experimental results of pump performance are shown in Fig. 3. The

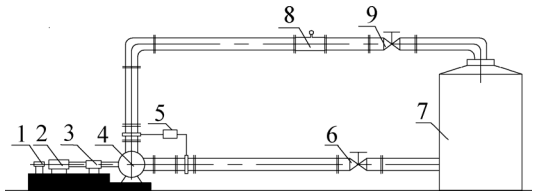

Fig. 2 Test bench: 1−Photoelectric encoder; 2−Motor; 3−Crankshaft bearing; 4−Centrifugal pump; 5−Pressure transmitter; 6−Inlet control valve; 7−Water box; 8−Electromagnetic flowmeter; 9−Outlet control valve

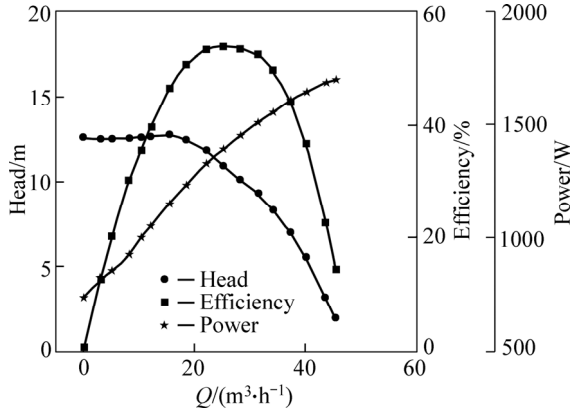

Fig. 3 Pump performance curves

experimental parameters can be got at the highest efficiency point. The discharge Q=25.2 m^3/h, the head H=10.9 m, the pump efficiency η=53.9%, the rotational speed n=1450 r/min, and the specific speed n_s=73.6.

2.3 PIV test

The PIV system applied in this experiment was the TSI model. It mainly included NewWave YAG200-NWL pulse laser, the 610035 laser pulse TM synchronizer, the 630059 power view^{TM} plus 4M PIV camera, Insight 3G, the 610015 light arm, light source lens, and so on. A typical PIV system configuration is given in Fig. 4.

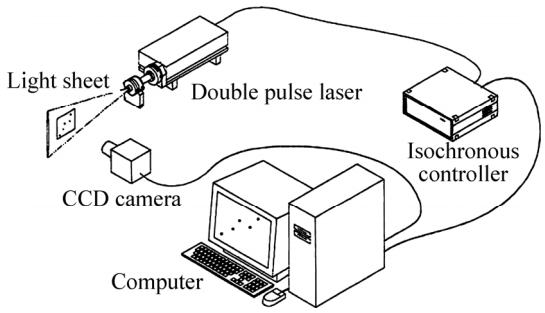

Fig. 4 Typical PIV system

The mid-plane of the impeller was selected as the investigation plane. Measurement region is illustrated in Fig. 5. Figure 6 presents the relative velocity distributions of experimental results inside the impeller under the design condition. There exist low velocity regions in some impeller passages and the velocity

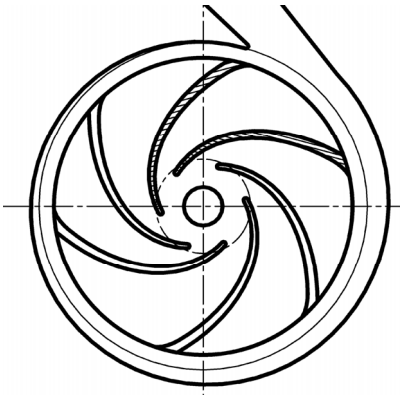

Fig. 5 Measurement region

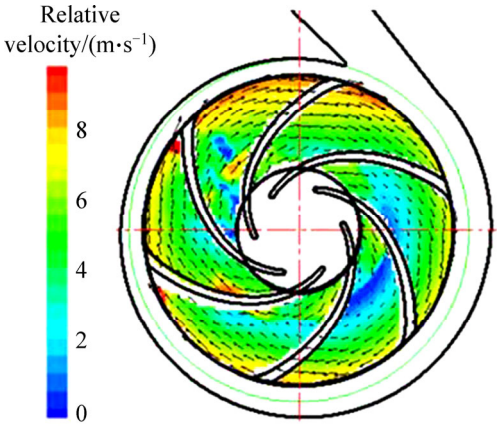

Fig. 6 Relative velocity distribution of impeller

increases with increasing the radius in most locations.

3 Numerical simulation

3.1 Numerical method

The ANSYS-CFX 12.1 was selected for the solution of 3D Navier-Stokes equation due to its characteristics of robust and fast convergence. The k−ε model was selected. The advection scheme was set to high resolution. The convergence criterion was 10^{-5}. The surface roughness of the wall within the control volume was set to be 50 μm. The inlet and outlet boundary conditions were set to normal speed inlet and opening Pres, and Dirn outlet. As the motion of the impeller blades relative to the stationary volute was focused in the investigation, the analysis must involve multiple frames of reference. The volute and outlet pipe were set in stationary frame and the impeller was set in rotary frame. The interfaces between two stationary components, rotary and stationary components were set to general grid and rotor stator interface, respectively.

3.2 Mesh generation

Three commonly implemented mesh styles were considered for a computation solution in centrifugal pump models (Fig. 7). All meshes in this work were

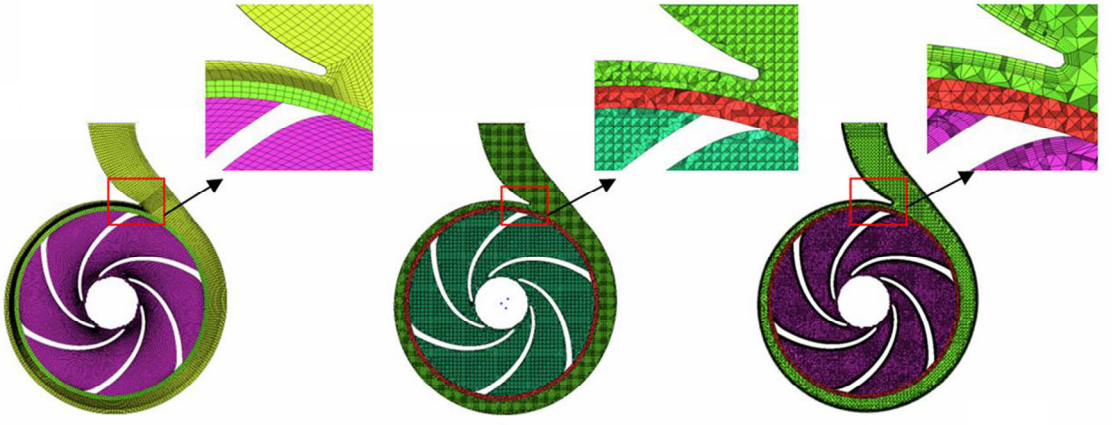

(a) (b) (c)

Fig. 7 Meshing styles of centrifugal pump model: (a) Structured mesh; (b) Unstructured mesh; (c) Hybrid mesh

created using the meshing program ICEM (ANSYS Inc.) and were refined based on the grid independence as analyzed in Ref. [19].

The structured meshes (Fig, 7(a)) consist of six-sided hexahedral elements arranged in a system of interconnected blocks. This multi-block structure is difficult to develop because gridlines may be distorted, but must remain continuous throughout the geometry. This means that the number of cells on mating block faces must match. Designing a qualified block-structured meshing configuration for a complex geometry such as centrifugal pump is an intensive nontrivial task of user. However, the solution quality resulting from hexahedral meshes is often considered to be superior to that from tetrahedral meshes with much more control volumes or elements. In addition, hexahedral meshes can be aligned with the predominant direction of the flow.

The unstructured tetrahedral meshing style (Fig. 7(b)) considered consists of four-sided elements. In comparison to structured meshes, tetrahedral meshes can be generated automatically by many commercial grid generation software packages. However, unstructured meshes are not capable of aligning with the direction of predominant flow, thereby increasing the numerical diffusion.

Recently, a number of commercial mesh generation packages have ability to develop hybrid grids consisting of multiple styles of elements. The most practical hybrid mesh style is employed which includes tetrahedral elements in the core of the flow surrounded by a layer of pyramid or hexahedral elements at the wall. And the hybrid tetrahedral/pyramid mesh is selected (Fig. 7(c)).

4 Grid convergence error

For complicated problems, the most reliable method for assessing the grid convergence (discretization) errors in the solution to partial differential equations was a posteriori method based on Richardson extrapolation [10]. ROACHE [8] has proposed the grid convergence index (GCI) as a uniform method for the results of grid refinement studies. As a minimum requirement for estimating solution accuracy, two grid solutions are employed to produce an error estimate. The methods [20] of calculating GCI based on Richardson extrapolation used are as follows.

When a differential equation is solved numerically on mesh level k (k=1, 2, 3, k for fine mesh is larger than that for coarse mesh),

$$f_2 = f_{\text{exact}} + g_p h_2^p + O(h_2^{p+1}) \tag{1}$$

$$f_1 = f_{\text{exact}} + g_p h_1^p + O(h_1^{p+1}) \tag{2}$$

$$f_3 = f_{\text{exact}} + g_p h_3^p + O(h_3^{p+1}) \tag{3}$$

where f_k is a discrete solution value on mesh level k, f_{exact} is the exact solution to the continuum partial differential equation, h_k is some measure of the grid spacing on mesh k, p is the order of discretization method, and g_p is the pth-order error term coefficient.

The grid refinement factor is defined as

$$r_{k,k+1} = \frac{h_k}{h_{k+1}} \tag{4}$$

Rigorously, grid convergence measures should be based on refining the grid by a factor of 2, i.e., grid halving. However, dividing hexahedral elements by a factor of 2 in three dimensions increases the total number of elements in the model by a factor of 8. Due to this order of magnitude increase in element count for successive grid refinements, it is not always practical to apply true grid halving. However, values are a function of the grid refinement factor, r, as well as the order of the method employed [21]. In general, grid reduction factors

less than r=2 are employed. The associated r-value is calculated as the ratio of control volumes in the fine to coarse meshes:

$$r_{k,k+1}=(\frac{N_{k+1}}{N_k})^{1/3} \tag{5}$$

where N_k is the number of control volumes in mesh level k.

The relative difference in two successive grid levels is defined as

$$\delta_{r(k,k+1)}=\left|\frac{f_k-f_{k+1}}{f_{k+1}}\right|=\left|\frac{\delta_{k,k+1}}{f_{k+1}}\right| \tag{6}$$

where $\delta_{k,k+1}=f_k-f_{k+1}$.

If the higher-order terms are neglected in Eqs. (1)−(3), then the preceding equations can be solved for approximations to the order p to give

$$\frac{\delta_{12}}{r_{12}^p-1}=\frac{\delta_{23}r_{23}^p}{r_{23}^p-1} \tag{7}$$

The GCI (G) is defined as

$$\begin{cases} G_{k+1}=F_{\mathrm{s}}\dfrac{\delta_{r(k,k+1)}}{r_{k,k+1}^{\mathrm{p}}-1} \\ G_k=F_{\mathrm{s}}\dfrac{r_{k,k+1}^p\delta_{r(k,k+1)}}{r_{k,k+1}^p-1} \end{cases} \tag{8}$$

The factor of safety, F_{s}, is generally selected to be 3. Then, the GCI can be calculated based on Eqs. (5)−(8).

5 Results

5.1 *w*/*u* distribution

To reveal the velocity distribution in impeller, region A is selected to study the distribution of w/u (where w is relative velocity and u is circumferential velocity) which is dimensionless (Fig. 8). The shooting effect is not ideal for some reasons. Therefore, the velocity distributions near the wall are neglected.

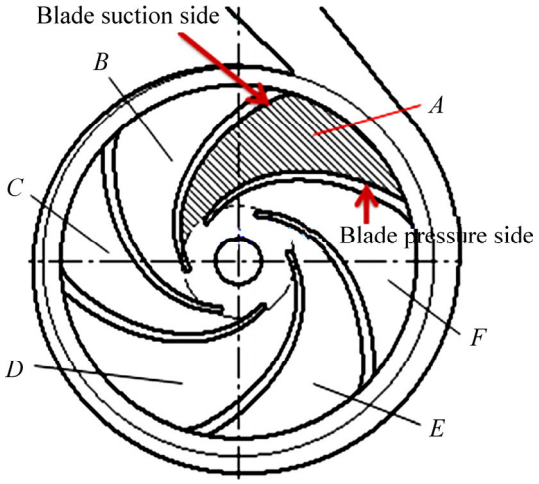

Fig. 8 Test region

The w/u distributions from blade pressure side to blade suction side at place 2 mm far away from impeller outlet in Region A are shown in Fig. 9. It can be seen that the value of w/u from blade pressure side to blade suction side in PIV experimental data reduces first and then increases. For the structured grid, the w/u-value changes twice in mesh for 5110000 cells, and four times for 1250000 and 2760000 cells (Fig. 9(a)), and its variation is different from the result of PIV test. For the unstructured grid and hybrid grid, the w/u-value

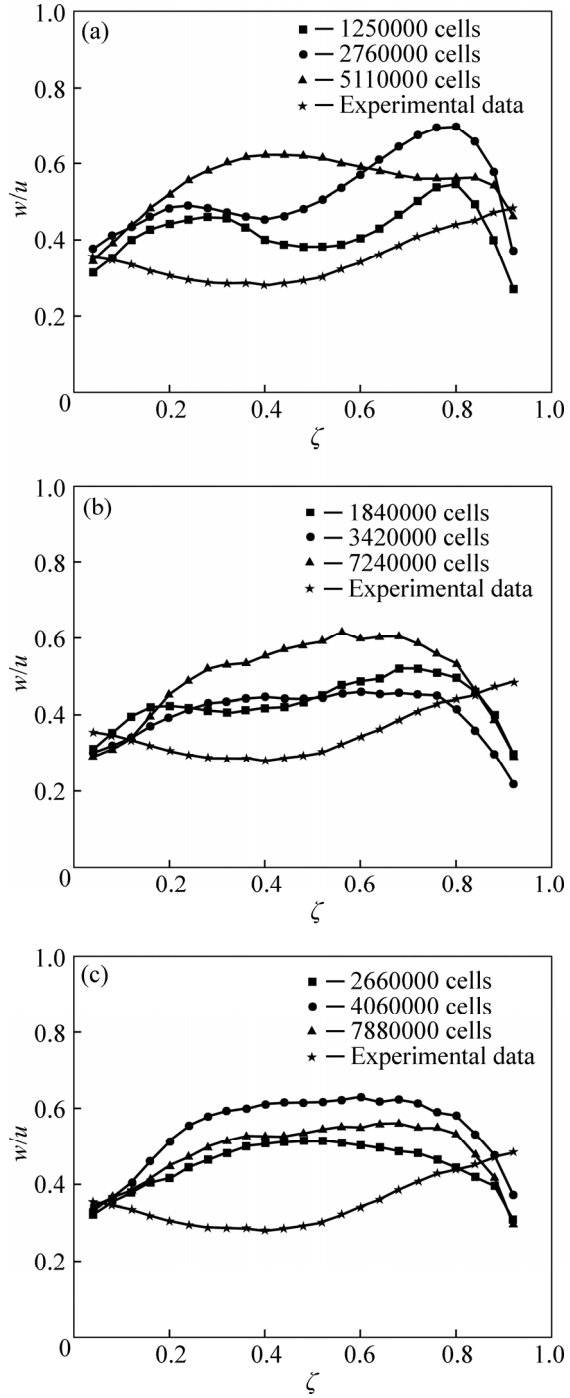

Fig. 9 w/u distributions from blade pressure side to blade suction side in Region A: (a) Structured hexahedral meshes; (b) Unstructured tetrahedral meshes; (c) Hybrid meshes

increases first and then reduces contrary to PIV test results (Figs. 9(b) and (c)). Nevertheless, whatever structured grid, unstructured grid or hybrid grid, there is certain difference for the value of *w/u* with the change of grid cell number. And for the artificial reason, PIV test error, etc, the simulation results have errors to different degrees compared with experimental data.

5.2 Grid convergence

Based on above comparisons, it is hard to accurately evaluate grid convergence. As such, quantitative measures of grid convergence such as p and GCI values are necessary. And grid convergence parameters have been evaluated for each of the three mesh styles considered. Comparisons between coarse and fine grids are considered within each style. Results of this comparison in the form of grid convergence values and required simulation times are reported in Tables 2−4 and are discussed below. Equations (1)−(8) are used to calculate the value of p and GCI which is calculated based on results of the variable head of centrifugal pump. That is to say, the f_k represents the calculated variable head for mesh level k.

Table 2 Grid convergence measured for structured grid

Grid size	p	GCI/%
1250000		9.40
2760000	2.50	2.93
5110000		2.09

Table 3 Grid convergence measured for unstructured grid

Grid size	p	GCI/%
1840000		20.65
3420000	2.32	9.16
7240000		7.3

Table 4 Grid convergence measured for hybrid grid

Grid size	p	GCI/%
2660000		11.11
4060000	2.28	4.21
7880000		4.14

The p-value is the order of discretization method. It should be the same for the three mesh styles. But the p calculated is an approximate value, so there must be difference. The p-values for structured, unstructured and hybrid grid are 2.50, 2.32, 2.28, respectively (Tables 2−4). They are close to each other.

For the structured hexahedral mesh, the GCI-value reduces with grid refinements (see Table 2). This means that the discretization error is the smallest for 5110000 cells among the three different numbers of structured meshes. And achieving a GCI of approximately 2% requires considering 5110000 hexahedral control volumes. For the unstructured tetrahedral mesh, grid refinements also result in a reduction of GCI value (see Table 3). The GCI-value for 7240000 cells is 7.3% which is larger than the smallest GCI-value of structured meshes. It needs to refine the grid for achieving the reduction of GCI. However, this mesh contains three times more control volumes than the hexahedral mesh. For hybrid mesh, GCI-value becomes smaller with increasing the grid cells (see Table 4). It needs to take the same measure compared with unstructured meshes for reducing the GCI-value. Refinement of the hybrid meshes is restricted by the requirement that the pyramid surface meshes should mate with the internal tetrahedral meshes at the wall boundary. Moreover, hybrid meshes that avoid element transitions near critical regions and that allow for better mesh refinement may provide improved results. In summary, the GCI-value for structured meshes is generally lower than that for the unstructured meshes and hybrid meshes. This means that the discretization error for the structured meshes is smaller.

5.3 Relative velocity streamlines distribution in impeller

Relative velocity streamlines and contours for different grid cells of three mesh styles are presented in Figs. 10−12. It is shown that the highest speed area is near the pump tongue where the flow velocity varies strongly. For the structured meshes, no vortex exists for 1250000 cells (Fig. 10(a)). And there is a vortex region in Region *A* for 2760000 cells and a vortex region both in Region *A* and Region *B* for 5110000 cells (Figs. 10(b) and (c)). For unstructured meshes, no vortex is shown in impeller mid-plane with the increase of grid cells (Fig. 11). For hybrid meshes, there is no vortex region for 1840000 cells and 3420 cells (Figs. 12(a) and (b)). But the vortexes appear in Region *E* when the level of grid is 7880000.

Comparisons of relative velocity distribution among different grid cells for three mesh styles allow for several general observations. First, more vortex regions may be captured with the refinement of grid. Then, except for the difference in vortex, the relative velocity distributions appear to be identical among three different numbers of grid cells for the same mesh style. Furthermore, among these three mesh styles, the streamline distributions have

a little difference and the vertex region may be shown in different impeller flow passages. And the structured meshes can get more vortex region in comparisons.

5.4 Velocity field in volute

The grids which have 5110000 cells, 7240000 cells and 7880000 cells, respectively, for structured, unstructured and hybrid meshes are chosen to study the velocity field in volute. Velocity vectors at mid-plane in volute and streamlines of secondary motion at Slice 1, 2 and 3 are presented in Fig. 13. Mid-plane velocity fields appear highly similar between the structured and unstructured meshes (Figs. 13(a) and (b)). Compared with structured and unstructured meshes, the hybrid meshes have a larger low-velocity area at outlet and some velocity which are opposite of the predominant velocity at Slice 2 (Fig. 13(c)). Secondary motions viewed at Slice 1 and 2 appear similar among these three mesh styles considered (Figs. 13(a)−(c)). And second vortex is observed at Slice 1. Minor difference exists at Slice 3 among the three mesh styles (Figs. 13(a)−(c)). There is only a single vortex for structured meshes but three vortexes and four vortexes, respectively, for unstructured and hybrid meshes.

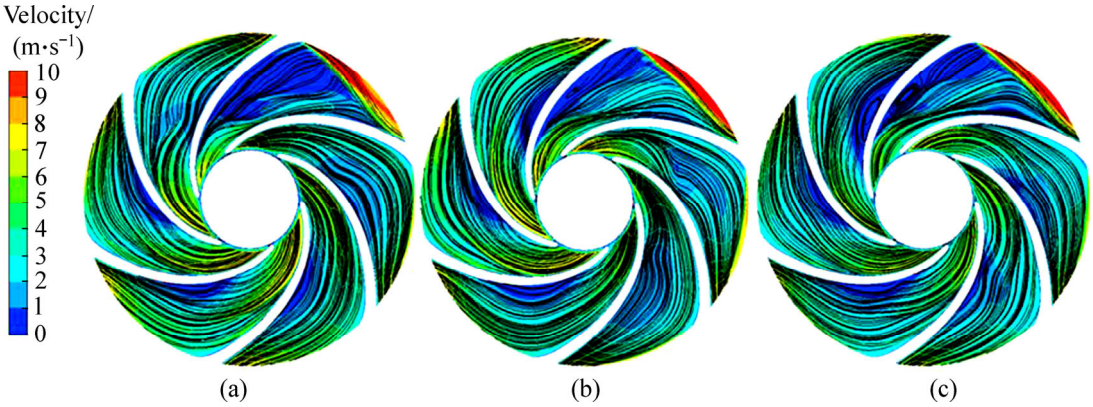

Fig. 10 Relative velocity streamlines and contours for structured meshes: (a) 1250000 cells; (b) 2760000 cells; (c) 5110000 cells

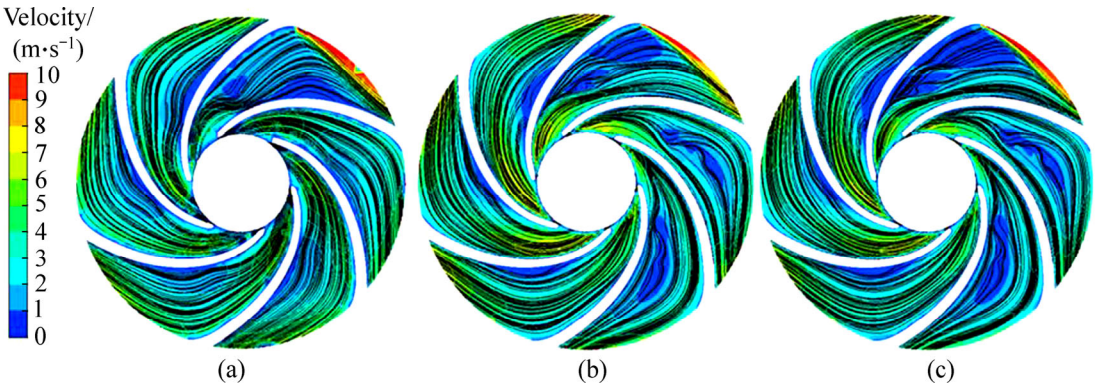

Fig. 11 Relative velocity streamlines and contours for unstructured meshes: (a) 1840000 cells; (b) 3420000 cells; (c) 7240000 cells

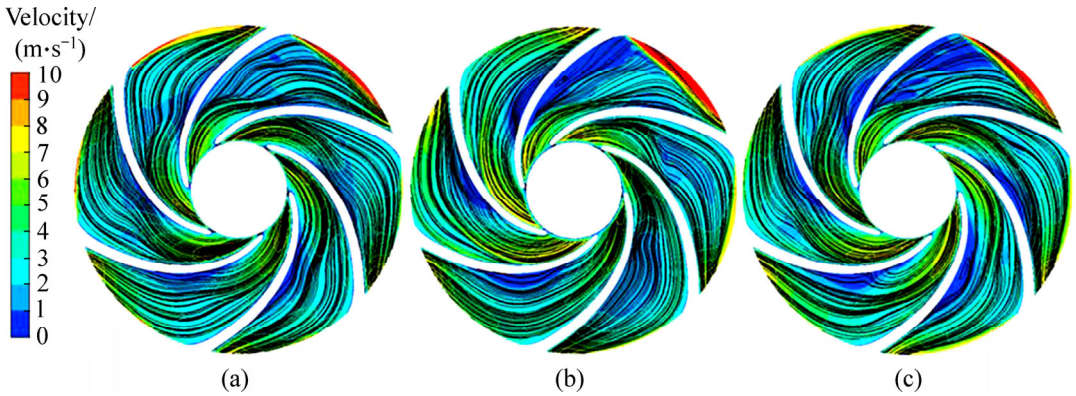

Fig. 12 Relative velocity streamlines and contours for hybrid meshes: (a) 2660000 cells; (b) 4060000 cells; (c) 7880000 cells

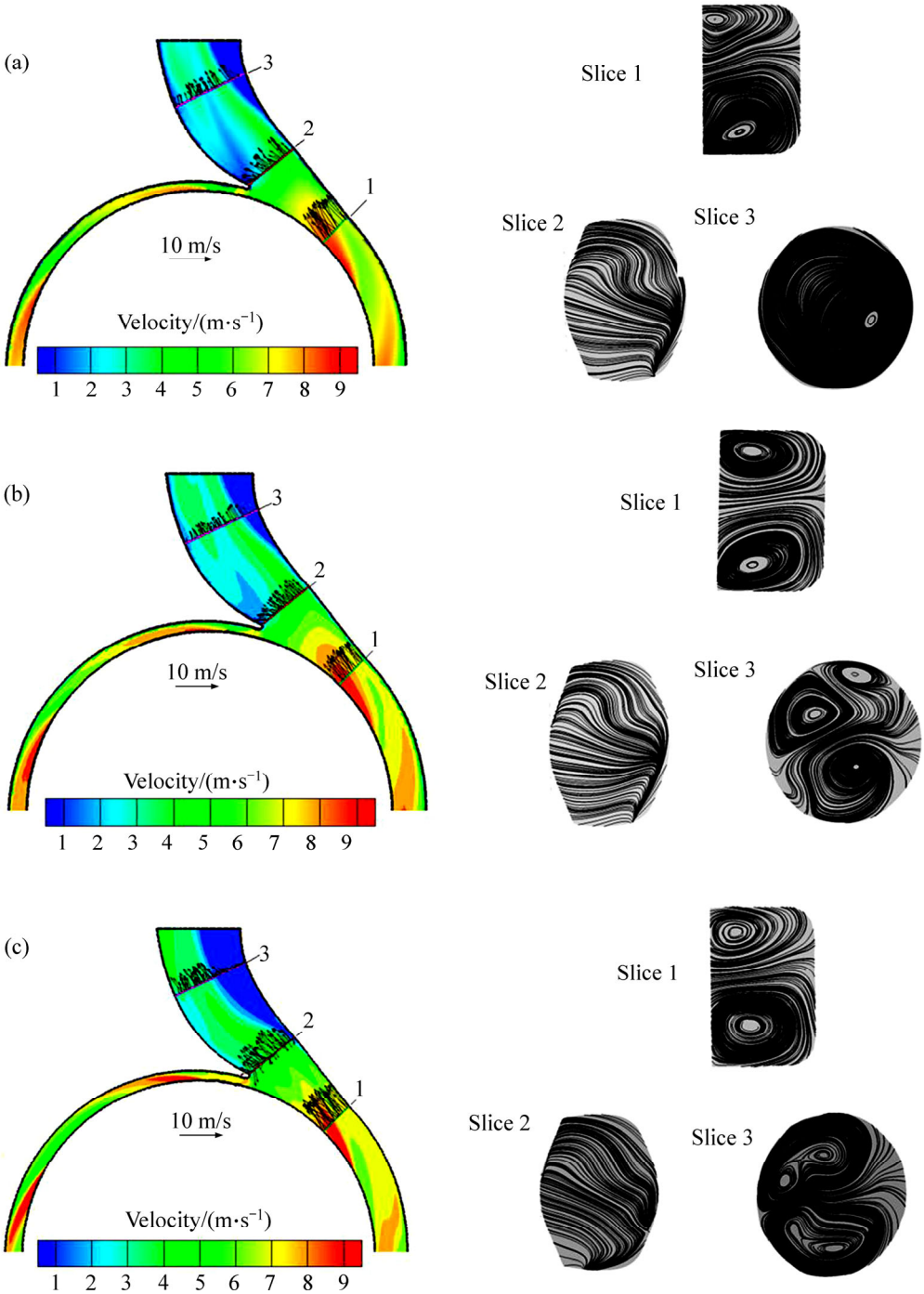

Fig. 13 Velocity vectors at mid-plane and streamlines at selected locations for pump model: (a) Structured meshes with 5100000 control volumes; (b) Unstructured meshes with 7240000 control volumes; (c) Hybrid meshes with 7880000 control volumes

6 Conclusions

1) The GCI-value for structured meshes is lower than that for unstructured and hybrid meshes when these three mesh styles have almost the same mesh level.

2) The simulation results for *w/u* distribution in these three mesh styles have errors to different degrees compared with experimental results. But the flow fields in most of the pump for the three mesh styles are qualitatively similar.

3) Minor difference exists in the vortex number in impeller passage for these three mesh styles, but the structured meshes can get more vortex region.

4) In the process of dealing with velocity distribution in volute mid-plane and secondary motions at some volute profiles, the hybrid meshes are found to have larger low-velocity area at outlet and more secondary vortexes at a specified location than structured meshes and unstructured meshes.

References

[1] DAI Cui, KONG Fan-yu, DONG Liang. Pressure fluctuation and its influencing factors in circulating water pump [J]. Journal of Central South University, 2013, 20: 149−155.

[2] DERAKHSHAN S, NOURBAKHSH A. Theoretical, numerical and experimental investigation of centrifugal pumps in reverse operation [J]. Experimental Thermal and Fluid Science, 2008, 32(8): 1620−1627.

[3] ZHU Xiao-hua, LI Jia-nan, TONG Hua. Mechanism analysis and process optimization of sand and plug removal with rotating jet in horizontal well [J]. Journal of Central South University, 2013, 20: 1631−1637.

[4] LIU Hou-lin, REN Yun, WANG Kai, WU Deng-hao, RU Wei-min, TAN Ming-gao. Research of inner flow in a double blades pump based on openfoam [J]. Journal of Hydrodynamics, 2012, 24: 226−334.

[5] Yl Qian. CFD Application in implantable Rotary blood pump design and validation [J]. Journal of Shanghai University (Natural Science), 2004, 10: 194−197. (in Chinese)

[6] CELIK I B, GHIA U, ROACHE P J. Procedure for estimation and reporting of uncertainty due to discretization in CFD applications [J]. Journal of Fluids Engineering, 2008, 130(7): 1−4.

[7] FREITAS C J. The issue of numerical uncertainty [J]. Applied Mathematical Modelling, 2002, 26(2): 237−248.

[8] ROACHE P J. Perspective: A method for uniform reporting of grid refinement studies [J]. Journal of Fluids Engineering, 1994, 116: 405−405.

[9] OBERKAMPF W L, TRUCANO T G. Verification and validation in computational fluid dynamics [J]. Progress in Aerospace Sciences, 2002, 38(3): 209−272.

[10] RICHARDSON L F. The approximate arithmetical solution by finite differences of physical problems involving differential equations, with an application to the stresses in a masonry dam [J]. Philosophical Transactions of the Royal Society of London. Series A, Containing Papers of a Mathematical or Physical Character, 1911, 210: 307−357.

[11] KARIMI M, AKDOGAN G, DELLIMORE K H, BRADSHAWA S M. Quantification of numerical uncertainty in computational fluid dynamics modelling of hydrocyclones [J]. Computers & Chemical Engineering, 2012, 43: 45−54.

[12] ELSAYED K, LACOR C. The effect of cyclone inlet dimensions on the flow pattern and performance [J]. Applied Mathematical Modeling, 2011, 35(4): 1952−1968.

[13] LIJO V, KIM H D, SETOGUCHI T. Analysis of choked viscous flows through a constant area duct [J]. Proceedings of the Institution of Mechanical Engineers, Part G: Journal of Aerospace Engineering, 2010, 224(11): 1151−1162.

[14] TANNEHILL J C, ANDERSON D D A, PLETCHER R H. Computational fluid mechanics and heat transfer [M]. Boca Raton: CRC Press, Taylor & Francis, 1997: 1−10.

[15] FERZIGER J H, PERIĆ M. Computational methods for fluid dynamics [M]. Berlin: Springer, 1996: 160.

[16] ZHOU Shui-qing, KONG Fan-yu, WANG Zhi-qiang, YI Chun-long, ZHANG Yong. Numerical simulation for low specific-speed centrifugal pump with structured grid [J]. Transactions of the Chinese Society of Agricultural Machinery, 2011, 42(7): 66−69. (in Chinese)

[17] LONGEST P, VINCHURKAR S. Effects of mesh style and grid convergence on particle deposition in bifurcating airway models with comparisons to experimental data [J]. Medical Engineering & Physics, 2007, 29(3): 350−366.

[18] LIU Y, PEKKAN K, JONES S C, YOGANATHAN A P. The effects of different mesh generation methods on computational fluid dynamic analysis and power loss assessment in total cavopulmonary connection [J]. Journal of Biomechanical Engineering, 2004, 126(5): 594−603.

[19] LIU Hou-lin, LIU Ming-ming, DONG Liang, DU Hui. Effects of grid types on numerical calculation accuracy of centrifugal pump [J]. Journal of Huazhong University of Science and Technology (Natural Science Edition), 2013, 41(10): 64−67. (in Chinese)

[20] ROY C J. Grid convergence error analysis for mixed-order numerical schemes [J]. AIAA Journal, 2003, 41(4): 595−604.

[21] ROACHE P J. Computational fluid dynamics [M]. Albuquerque: Hermosa, 1976: 286−287.

(Edited by YANG Bing)